ORMIR_XCT: A Python package for high resolution peripheral quantitative computed tomography image processing

Michael T. Kuczynski [1,2*], **Nathan J. Neeteson**[1,2*], **Kathryn S. Stok** [3], **Andrew J. Burghardt** [4], **Michelle A. E. Espinosa** [3,5,6], **Jared Vicory** [7], **Justin J. Tse** [1,8], **Pholpat Durongbhan** [3], **Serena Bonaretti** [9], **Andy Kin On Wong** [6,10], **Steven K. Boyd** [1,8], **and Sarah L. Manske** [1,8¶]

1 McCaig Institute for Bone and Joint Health, Cumming School of Medicine, University of Calgary, Calgary, Canada **2** Department of Biomedical Engineering, Schulich School of Engineering, University of Calgary, Calgary, Canada **3** Department of Biomedical Engineering, The University of Melbourne, Parkville, Australia **4** Department of Radiology and Biomedical Imaging, University of California, San Francisco, USA **5** Rehabilitation Sciences Institute, The University of Toronto, Toronto, Canada **6** Joint Department of Medical Imaging, University Health Network, Toronto, Canada **7** Kitware, Inc., Carrboro, North Carolina, USA **8** Department of Radiology, Cumming School of Medicine, University of Calgary, Calgary, Canada **9** Swiss Center for Musculoskeletal Imaging, Balgrist Campus, Zurich, Switzerland **10** Department of Epidemiology, Dalla Lana School of Public Health, University of Toronto, Toronto, Canada **¶** Corresponding author ***** These authors contributed equally.

1 − Statement of need:

High resolution peripheral quantitative computed tomography (HR-pQCT) is an imaging technique with a nominal isotropic voxel size of 61μm capable of imaging trabecular bone *in-vivo*. HR-pQCT has a wide range of applications, primarily focused on bone to improve our understanding of musculoskeletal diseases (K. Brunet S. C., 2020), assess epidemiological associations (Burt, 2016), and evaluate the effects of pharmaceutical interventions (T. Brunet S. C., 2021). Processing HR-pQCT images has largely been supported using the scanner manufacturer's scripting language (Image Processing Language, IPL, Scanco Medical). However, by expanding image processing workflows outside of the scanner manufacturer's software environment, users have the flexibility to apply more advanced mathematical techniques and leverage modern software packages to improve image processing. The ORMIR_XCT Python package was developed to reimplement some existing IPL workflows and provide an open and reproducible package allowing for the development of advanced HR-pQCT data processing workflows.

2 − Package summary:

The development of this package began during the Jupyter Community Workshop in Maastricht, Netherlands in June 2022, hosted by the Open and Reproducible Musculoskeletal Imaging Research (ORMIR) group. During this workshop, the conceptualization and initial development of the ORMIR_XCT package began with support from Kitware. The ORMIR_XCT package is currently being used by members of the ORMIR community to assess bone mineral density (BMD) and joint space width (JSW) changes in HR-pQCT scans of patients with osteoarthritis or rheumatoid arthritis.

The ORMIR_XCT package contains four modules for processing HR-pQCT data of bones and

41 joints: 1) automatic contouring of the periosteal surface, 2) JSW analysis, 3) BMD calculation,
42 and 4) segmentation of trabecular bone. Analyses have been performed to compare outputs
43 from the ORMIR_XCT package to results generated using IPL. Jupyter Notebook examples are
44 provided to describe the workflows implemented in the ORMIR_XCT package.

45 3 − Comparison to IPL:

46 3.1 - Autocontour:

47 Automatic periosteal contouring (autocontour) was performed on a sample dataset of HR-pQCT
48 images of the 2nd and 3rd distal interphalangeal (DIP) and trapeziometacarpal (TMC) joints (n
49 = 59). The images came from 10 participants in an osteoarthritic group and 10 participants in
50 a control group. This dataset is representative of typical data that is collected using HR-pQCT.
51 Binarized images were obtained using both the IPL standard method for automatic periosteal
52 contouring (Burghardt, 2010) and the ORMIR_XCT package. Segmentation were compared by
53 computing DICE coefficients, Jaccard indices, and Hausdorff distances between images. The
54 IPL method for automatic periosteal contouring was taken as the ground truth. Results of the
55 segmentation comparison are shown in Figure 1.

Scan	DIP2				DIP3				TMC			
	DICE	Jaccard	Mean Hausdorff (voxels)	Maximum Hausdorff (voxels)	DICE	Jaccard	Mean Hausdorff (voxels)	Maximum Hausdorff (voxels)	DICE	Jaccard	Mean Hausdorff (voxels)	Maximum Hausdorff (voxels)
1	0.97	0.94	0.05	10.68	0.98	0.96	0.03	9.06	0.98	0.96	0.06	21.02
2	0.96	0.92	0.06	7.81	0.94	0.89	0.15	18.68	0.98	0.97	0.04	19.03
3	0.97	0.94	0.05	8.12	0.97	0.93	0.07	17.32	0.98	0.96	0.06	25.67
4	0.96	0.93	0.06	10.05	0.98	0.96	0.03	9.11	0.95	0.91	0.26	37.36
5	0.97	0.94	0.06	10.49	0.97	0.94	0.05	12.41	0.98	0.96	0.07	22.67
6	0.96	0.93	0.07	12.37	0.96	0.92	0.08	14.73	0.99	0.97	0.03	20.61
7	0.98	0.97	0.02	6.40	0.99	0.98	0.01	3.61	0.98	0.96	0.08	26.32
8	0.97	0.93	0.06	20.62	0.98	0.96	0.04	13.34	0.94	0.89	0.51	45.29
9	0.98	0.97	0.02	9.70	-	-	-	-	0.98	0.95	0.06	21.21
10	0.98	0.96	0.03	8.60	0.97	0.95	0.04	18.00	0.96	0.91	0.23	33.73
11	0.98	0.96	0.03	5.48	0.99	0.97	0.02	8.06	0.99	0.97	0.03	22.14
12	0.97	0.94	0.05	9.00	0.96	0.92	0.09	27.29	0.97	0.95	0.09	22.00
13	0.98	0.96	0.02	9.00	0.98	0.96	0.03	8.60	0.97	0.95	0.09	21.66
14	0.98	0.96	0.03	6.00	0.99	0.97	0.02	7.28	0.99	0.97	0.03	17.92
15	0.98	0.95	0.04	14.87	0.98	0.97	0.02	7.68	0.99	0.97	0.02	18.11
16	0.96	0.93	0.07	10.68	0.99	0.97	0.02	7.00	0.99	0.97	0.03	18.14
17	0.99	0.98	0.02	6.16	0.98	0.97	0.03	9.43	0.99	0.98	0.03	23.26
18	0.99	0.98	0.01	4.47	0.99	0.98	0.01	4.90	0.99	0.97	0.03	15.30
19	0.98	0.97	0.02	4.24	0.99	0.97	0.02	23.60	0.99	0.97	0.03	22.20
20	0.98	0.96	0.04	11.75	0.99	0.97	0.02	4.36	0.99	0.97	0.04	24.45

Figure 1: Table 1: DICE coefficients, Jaccard indices, and Hausdorff distances (voxels) between IPL and ORMIR_XCT automatic contouring implementations. All scans were obtained from a second-generation HR-pQCT scanner (XtremeCT2, Scanco Medical) with an isotropic voxel size of 61µm. DIP2: 2nd distal interphalangeal joint, DIP3: 3rd distal interphalangeal joint, TMC: trapeziometacarpal joint.

56 3.2 - Thickness:

57 The ORMIR_XCT package contains an open-source implementation of the algorithm for model-
58 independent thickness estimation by Hildebrand *et al* (Hildebrand & Ruegsegger, 1996). This
59 thickness estimation is used to compute several morphological measurements from HR-pQCT
60 images, including trabecular thickness, trabecular separation, and cortical thickness. Given
61 a binary mask describing a three-dimensional object as input, the algorithm first computes
62 the distance map (via a distance transform), describing at each voxel the radius of the largest
63 sphere centered at that voxel that is entirely within the object. Next, the local thickness map
64 is computed by iterating through all voxels in the mask and assigning them a local thickness
65 value that is the diameter of the largest sphere in the distance map that contains that voxel.
66 The thickness of a structure can then be computed as the volume-weighted mean of the local
67 thickness map, with optional adjustments for a minimum thickness value if desired to reduce
68 the effect of surface noise.

69 Hildebrand & Ruegsegger (1996) note an optimization for the algorithm where first, the distance
70 ridge (also known as skeletonization or medial axis) is computed and only the distance map
71 values on the distance ridge are used for local thickness map computation. We implemented
72 this optimized version of the algorithm with NumPy (v1.23.3) (Harris, 2020) and Numba
73 (v0.56.3) (Lam, 2015). Finally, we have noted and compensated for a discrepancy between
74 the definition of the distance map by Hildebrand & Ruegsegger (1996) and the outputs of
75 many common open-source distance map algorithms (including those available in SimpleITK
76 (v2.0.2) (Lowekamp, 2013) and scikit-image (v0.19.2) (Van der Walt, 2014)). Hildebrand &
77 Ruegsegger (1996) define their distance map as "the radius of the largest sphere centered at
78 the point and still completely inside the structure". In contrast, most other distance transforms
79 compute the distance from the center of a voxel inside the mask to the nearest voxel center
80 outside the mask.

81 To compensate for this, we developed an oversampling distance transform function (Figure 2).
82 In this function, an input mask is up-sampled to double the voxel size, and a sequence of
83 morphological filters are applied to ensure that the newly introduced voxels on the boundary
84 between the structure and the background are assigned as background voxels. A distance
85 transform is applied to this mask, resulting in a distance map where the spheres fit entirely
86 within the structure defined by the mask, and the resulting distance map is down-sampled to
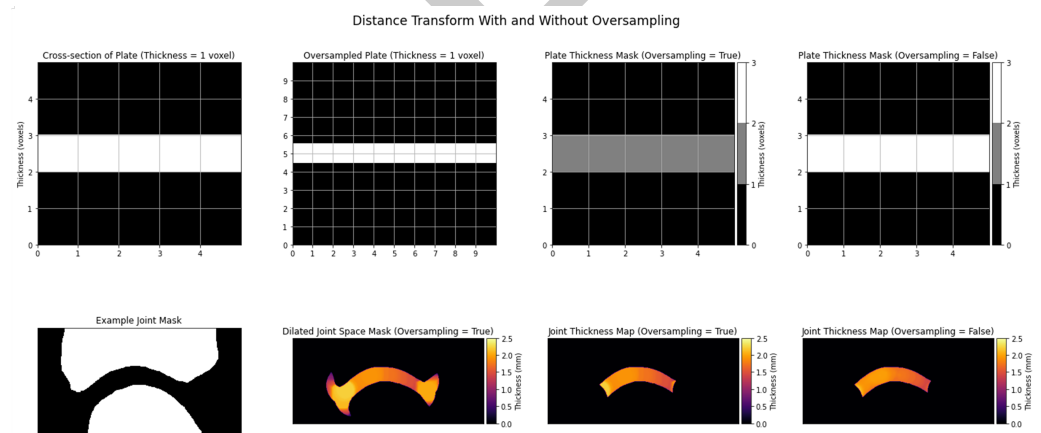87 the original voxel size.

Figure 2: Figure 1: Examples of the thickness estimation algorithm implemented in the `ORMIR_XCT` package. Top row: thickness calculation on a 1 voxel thick plate demonstrating how thickness estimation is improved using the oversampling distance transform function (thickness = 1 voxel using oversampling, thickness = 2 voxels without oversampling). Bottom row: thickness calculation applied to a sample finger joint.

88 The user is given a choice, via a Boolean flag parameter in the compute_local_thick-
89 ness_from_mask and calc_structure_thickness_statistics functions, to use the oversampling
90 distance transform for thickness estimation. The choice is given because different users
91 may have variable preferences in applying alternate definitions regarding the bounds of their
92 structures (whether they be contained within the mask voxels or extend to the center of the
93 neighbouring background voxels) and because using the normal (*i.e.*, not oversampled) distance
94 transform will provide better congruence with thickness calculations produced using IPL.

95 To evaluate the thickness computation implemented in the `ORMIR_XCT` package, a set of
96 synthetic shapes were generated to simulate bones of varying sizes. These shapes include solid
97 and hollow spheres, solid and hollow cylinders, and plates of varying thicknesses (Kuczynski,
98 2023). The standard IPL joint space width (JSW) analysis workflow (Stok, 2020) was per-
99 formed on the synthetic shape dataset using the following parameters: ridge_epsilon = 0.9,
100 assign_epsilon = 1.8, suppress_boundary = 0, and version = 3. This set of parameters

is currently used for JSW analysis of *in vivo* finger joints. ORMIR_XCT thickness was calculated using the oversampling distance transform function described above. Bland-Altman plots were generated to compare thickness results between algorithms (Figure 3).
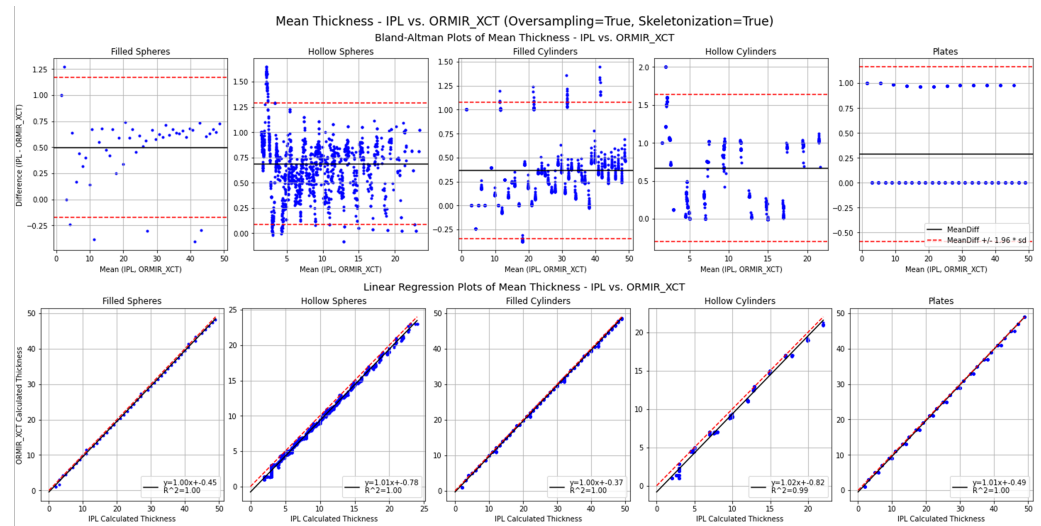

Figure 3: Figure 2: Bland-Altman and regression plots of mean joint space thickness computed using IPL and the `ORMIR_XCT` package . Top row: black lines indicate mean difference and red dotted line shows the limits of agreement. Bottom row: solid black line indicates the linear regression between IPL and ORMIR_XCT computed thickness and red dotted lines indicate a line of unity.

3.3 – Bone mineral density:

Images obtained from HR-pQCT scanners are saved using the manufacturer's proprietary file format (AIM). To process HR-pQCT images using Python, these files need to be converted to a file format that can be interpreted by common image processing Python libraries. The `ITKIOScanco` module is used in the `ORMIR_XCT` package to convert HR-pQCT images to other common medical image file types. However, the `ITKIOScanco` module converts HR-pQCT images to Hounsfield Units (HU) by default. Measures of BMD require the image to be calibrated in density units (mg of hydroxyapatite per cm3). Several image unit conversions have been included in the `ORMIR_XCT` package to allow for conversion between HR-pQCT native units (termed Scanco units) and each of HU, density, and linear attenuation units. A sample dataset of HR-pQCT images of second and third metacarpal phalangeal (MCP) joints (n = 292) was used to compare BMD results between IPL and the `ORMIR_XCT` package. BMD was reported separately for the distal (DST) and proximal (PRX) segments of each joint (Figure 4).
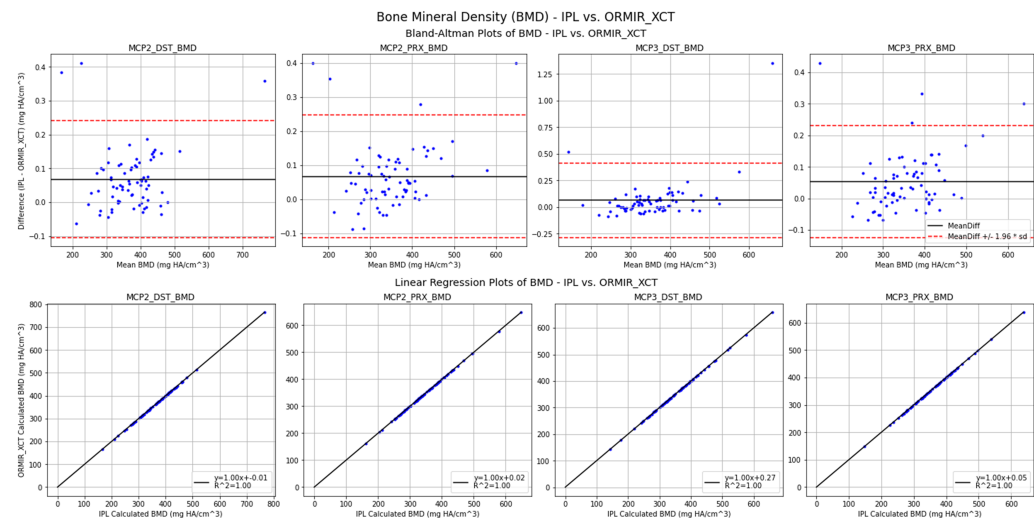
Figure 4: Figure 3: Bone mineral density (mg HA/cm3) linear regression and Bland-Altman plots comparing IPL and the ORMIR_XCT computed bone mineral density (BMD). All scans were obtained from a second-generation HR-pQCT scanner (XtremeCT2, Scanco Medical) with an isotropic voxel size of 61µm. MCP2: 2nd metacarpal phalangeal joint, MCP3: 3rd metacarpal phalangeal joint, DST: distal, PRX: proximal.

3.4 - Trabecular segmentation:

A common operation performed in IPL is the application of a Gaussian smoothing filter followed by a global threshold-based image segmentation. The gauss_seg function in IPL has been reimplemented in the ORMIR_XCT package and the similarity of IPL and ORMIR_XCT trabecular segmentations were computed using DICE coefficients, Jaccard indices, and Hausdorff distances (Figure 5). The same dataset used to test the automatic contouring module was used to compare IPL and ORMIR_XCT trabecular segmentation.

Scan	DIP2				DIP3				TMC			
	DICE	Jaccard	Mean Hausdorff (voxels)	Maximum Hausdorff (voxels)	DICE	Jaccard	Mean Hausdorff (voxels)	Maximum Hausdorff (voxels)	DICE	Jaccard	Mean Hausdorff (voxels)	Maximum Hausdorff (voxels)
1	0.99	0.98	0.01	16.55	0.99	0.97	0.02	16.25	0.99	0.98	0.02	40.16
2	0.99	0.98	0.02	10.10	0.99	0.97	0.02	11.36	0.99	0.98	0.01	19.34
3	0.99	0.98	0.01	9.22	0.99	0.98	0.01	12.21	0.99	0.98	0.02	37.66
4	0.99	0.98	0.01	13.49	0.99	0.98	0.01	11.36	0.99	0.97	0.03	36.46
5	0.99	0.98	0.01	22.11	0.99	0.98	0.01	18.00	0.99	0.98	0.02	32.40
6	0.99	0.97	0.02	13.19	0.99	0.98	0.02	16.31	0.99	0.98	0.02	29.00
7	0.99	0.99	0.01	8.54	0.99	0.99	0.01	8.06	1.00	0.99	0.01	23.22
8	1.00	0.99	0.01	10.30	0.99	0.99	0.01	15.03	1.00	0.99	0.01	33.62
9	0.99	0.99	0.01	5.83	-	-	-	-	1.00	0.99	0.01	35.18
10	0.99	0.99	0.01	10.63	0.99	0.99	0.01	9.43	1.00	0.99	0.01	30.50
11	0.99	0.99	0.01	9.00	0.99	0.99	0.01	9.95	1.00	0.99	0.01	31.95
12	0.99	0.98	0.01	9.49	1.00	0.99	0.01	15.59	0.99	0.98	0.01	21.28
13	0.99	0.99	0.01	13.75	0.99	0.99	0.01	13.15	0.99	0.98	0.05	36.94
14	0.99	0.98	0.01	9.64	0.99	0.99	0.01	11.66	1.00	0.99	0.02	18.38
15	0.99	0.99	0.01	13.19	0.99	0.99	0.01	12.73	0.99	0.99	0.03	33.20
16	0.99	0.99	0.01	17.49	0.99	0.99	0.01	11.05	1.00	0.99	0.01	23.15
17	0.99	0.99	0.01	5.92	0.99	0.99	0.01	6.63	1.00	1.00	0.00	27.22
18	0.99	0.99	0.01	8.37	0.99	0.99	0.01	9.95	1.00	0.99	0.01	24.92
19	0.99	0.99	0.01	12.33	0.99	0.99	0.01	12.08	1.00	0.99	0.02	29.68
20	0.99	0.99	0.01	8.06	0.99	0.99	0.01	7.87	1.00	0.99	0.01	25.81

Figure 5: Table 2: DICE scores, Jaccard indices, and Hausdorff distances (voxels) for comparison of trabecular segmentation performed using IPL versus the ORMIR_XCT package. All scans were obtained from a second-generation HR-pQCT scanner (XtremeCT2, Scanco Medical) with an isotropic voxel size of 61µm. For each algorithm, Gaussian smoothing was performed with sigma = 0.5. Subsequently, segmentation was performed with lower and upper thresholds of 1,170 and 10,000 HU, respectively. DIP2: second distal interphalangeal joint, DIP3: third distal interphalangeal joint, TMC: trapeziometacarpal joint.

References:

Brunet, K., S. C. (2020). The utility of multi-stack alignment and 3D longitudinal image registration to assess bone remodeling in rheumatoid arthritis patients from second generation HR-pQCT scans. *BMC Medical Imaging*. https://doi.org/10.1186/s12880-020-00437-8

Brunet, T., S. C. (2021). Heterogenous bone response to biologic DMARD therapies in rheumatoid arthritis patients and their relationship to functional indices. *Scandinavian Journal of Rheumatology*. https://doi.org/10.1080/03009742.2020.1869303

Burghardt, B., A. J. (2010). Reproducibility of direct quantitative measures of cortical bone microarchitecture of the distal radius and tibia by HR-pQCT. *Bone*. https://doi.org/10.1016/j.bone.2010.05.034

Burt, L., L. A. (2016). Sex- and Site-Specific Normative Data Curves for HR-pQCT. *Journal of Bone and Mineral Research*. https://doi.org/10.1002/jbmr.2873

Harris, M., C. R. (2020). Array programming with NumPy. *Nature*. https://doi.org/10.1038/s41586-020-2649-2

Hildebrand, T., & Ruegsegger, P. (1996). A new method for the model-independent assessment of thickness in three-dimensional images. *Journal of Microscopy*. https://doi.org/10.1046/j.1365-2818.1997.1340694.x

Kuczynski, M. T. (2023). Synthetic shapes for ORMIR_XCT thickness measurement validation. In *Zenodo*. Zenodo. https://doi.org/10.5281/zenodo.8155738

Lam, P., S. K. (2015). Numba: A llvm-based python jit compiler. *Proceedings of the Second Workshop on the LLVM Compiler Infrastructure in HPC*. https://doi.org/10.1145/2833157.2833162

Lowekamp, C., B. C. (2013). The Design of SimpleITK. *Frontiers in Neuroinformatics*. https://doi.org/10.3389/fninf.2013.00045

Stok, B., K. S. (2020). Consensus approach for 3D joint space width of metacarpophalangeal joints of rheumatoid arthritis patients using high-resolution peripheral quantitative computed tomography. *Quantitative Imaging in Medicine and Surgery*. https://doi.org/10.21037/qims.2019.12.11

Van der Walt, S., S. (2014). scikit-image: image processing in Python. *PeerJ*. https://doi.org/10.7717/peerj.453